The Design of an Optimum System for Monitoring the Operational Status of a Spacecraft

Marvin Simon, Victor Vilnrotter, Alex Mileant, Sami 1 linedi
Jet Propulsion 1 aboratory
4800 Oak Grove 1 Drive
Pasadena, CA 91109

-Abstract

The design of a spacecraft monitoring system based on a Neyman-Pearson detection criterion is discussed. Each noncatastrophic state of the spacecraft is indicated by the transmission of a specific signal to the ground station. Complete failure of the spacecraft is indicated by the transmission of no signal. The set of signals chosen to represent the spacecraft states consists of a group of orthogonally spaced (in frequency) carriers each with unknown (random) phase. Receiver structures derived from maximum-likelihood considerations are proposed that provide suitable performance in the presence of frequency uncertainty (due to Doppler) and frequency rate uncertainty (due to oscillator drift). Numerical results are obtained from a combination of analysis anti simulation and indicate the tradeoffs among the various receiver structures between performance anti implementation complexity.

The Design of an Optimum System for Monitoring the Operational Status of a Spacecraft

Marvin Simon, Victor Vilnrotter, Alex Mileant, Sami Hinedi
Jet Propulsion Laboratory
4800 Oak Grove Drive
Pasadena, CA 91109

1. Introduction

The design of an optimum carrier communication system for monitoring the operational status (state) of an orbiting spacecraft is best handled by applying the principles of ll]axi~~~~ll~~-like'lil~ <~(>d detection used in hypothesis testing problems. in particular, each state of the spacecraft, e.g., spacecraft is fine, spacecraft has failed, spacecraft needs immediate attention, etc., is assigned a hypothesis and basal on an appropriately defined performance criterion, the receiver should be designed to minimize the required power-to-noise ratio (or energy-to-noise ratio when fixing observation time) needed to faithfully detect the hypothesis currently in effect.

in a hypothesis testing problem of the type described above, the notion of cost is particularly appropriate. For example, the cost of an error in deciding that the spacecraft is fine when indeed it has failed is much larger than the cost of an error in deciding that it needs immediate help when indeed it might only need help at a later time. Also, the probabilities associated with the hypotheses that represent the various spacecraft states are, in general, quite unequal, e.g., the probability of complete spacecraft failure is significantly less than the probability that it might need some particular form of help,

If a reasonable set of a priori hypothesis probabilities representing the spacecraft states are available and if an appropriate cost matrix (the ijth element of which is the cost associated with an error in deciding hypothesis H_j when in reality H_i is true) can be assigned, then the best criterion to apply is the so-called *minimum* risk or *Bayes criterion* wherein one attempts to minimize the risk, i.e., the average (statistical) cost.

More often than not, the a priori hypothesis probabilities are not known to the receiver and if they are, one can only estimate (approximate) their values from reliability studies performed on the spacecraft. Furthermore, an appropriate cost matrix might be difficult to construct anti indeed might be mission-dependent. In view of this, a so- called *Neyman-Pearson criterion* is often applied to such hypothesis testing problems wherein one maximizes the *probability of correct*

detection for a given *probability of false alarm* without the need for such a priori probability or cost information. Most applications of this criterion found in the literature are for the two hypothesis case since there', the notions of correct detection and false alarm are well-defined in terms of the signal present versus signal absent concept, While it is possible to extend this criterion to more than two hypotheses, the literature is essentially devoid of this discussion. The primary reason for this is as follows. While the notion of false alarm can still be meaningfully defined, i.e., deciding on *any of the* other *hypotheses corresponding to a signal present when indeed signal* is *absent (spacecraft* is *dead),* the notion of correct detection is somewhat ambiguous since there are now many possible signal present hypotheses to decide upon; hence there are many correct detection probabilities -- one associated with each of the signal present hypotheses.

Regardless of whether a Bayes or Neyman-Pearson criteria is selected, the optimum receiver *structure* that results will be independent of the correlation properties of the signals which represent the various spacecraft states. (Of course, the *performance* of the receiver will indeed depend on the signal correlation properties and thus a second consideration in the design of an optimum system (transmitter/receiver) is to choose that signal set which optimizes the system performance *for the given structure determined from the decision criteria applied.)* On the other hand, the' *specific implementation* of the optimum receiver structure depends heavily on the amount of information known about the parameters that characterize the received signals, e.g., their phase, carrier frequency, etc. For example, if all signal parameters (e. g., carrier phase, frequency, etc.) are known, then the optimum receiver takes the form of some type of coherent receiver which may or may not include a priori probability and cost information depending on the decision criterion adopted. At the other extreme, in the absence of any specific knowledge about the signal parameters, e.g., the carrier phase is assumed to be uniformly distributed in the interval $(-\pi,\pi)$, then the optimum receiver is a form of *noncoherent* receiver in that no attempt is made to estimate the carrier phase. Finally, a compromise between totally known and totally unknown parameter information, e.g., the carrier phase is characterized by a known probability density function, yields a form of *partially-coherent* receiver.

in this paper, we discuss only the design of a spacecraft monitoring system based on a Neyman-Pearson criterion. We begin with a brief discussion of this criterion as applied to multiple (more than two) hypothesis testing. The resulting

[1] In the spacecraft monitoring problem, one of the hypotheses (corresponding to complete spacecraft failure) still corresponds to signal absent; however, the presence of several different spacecraft states necessitates several different signal present hypotheses each characterized by its own unique signal.

test shall then form the basis of many of the receiver structures that follow.

2. A Neyman-Pearson Test for M Hypotheses

Consider a multiple hypothesis test in which the received signal $r(t)$ is characterized as follows:

$$t\text{“(t)} : \begin{cases} /1(1); & H_0 \\ s_i(1) + n(t); & H_i, i = 1,2,\ldots, \text{M- 1} \end{cases} \tag{1}$$

where $n(t)$ denotes the additive channel Gaussian noise with single-sided power spectral density N_0 w / 1 Iz, and $s_i(t)$, $i = 1,2,\ldots, M-1$ denotes the signals assigned to the noncatastrophic (other than complete failure) spacecraft states. Assuming that the noise only condition (null hypothesis H_0) is indeed true then deciding in favor of $s_i(1) + n(t)$ (hypothesis $H_i, i: 1,2,\ldots,M-1$) results in a false alarm. Since all of these false alarm conditions come about from the same conditional hypothesis (namely, H_0), it is logical to define the false alarm probability P_{FA} by

$$P_{FA} = \sum_{i=1}^{M-1} \Pr\{H_i | H_0\} \tag{2}$$

Characterizing $r(t)$ in terms of a vector observable r corresponding to the coefficients in its Karhunen-Loeve expansion (a special case of which could be the sampling expansion) and denoting by R_i, $i = 0, 1,\ldots M-1$ the set of disjoint regions in r-space corresponding to choosing in favor of $H_i, i: 1,2,\ldots, M-1$, then (2) can be expressed as

$$P_{FA} = \sum_{i=1}^{M-1} \int_{R_i} p(\mathbf{r}|H_0)d\mathbf{r} = 1 - \int_{R_0} p(\mathbf{r}|H_0)d\mathbf{r} \tag{3}$$

where $p(\mathbf{r}|H_0)$ is the conditional probability density function (pdf) of the vector observable r given the null hypothesis H_0.

Assuming that H_i is indeed true, then deciding in favor of s,(1)+ $n(t)$ results in a correct decision. We denote the probability of this event by

$$P_{Di} = \Pr\{H_i | H_i\} = \int_R p(\mathbf{r}|H_i)d\mathbf{r}, \qquad i = 1,2,\ldots, \text{M- 1} \tag{4}$$

In a two-hypothesis problem, i.e., $M = 2$, where there is only one correct detection probability, namely, $P_{D1} = \Pr\{H_1|H_1\} \triangleq P_D$, the Neyman-Pearson test is derived from the criterion of maximizing P_D subject to a constraint on P_{FA}. Note that this is meaningful and can be achieved independent of the knowledge of the a priori probabilities of H_0 and H_1. While in the *M hypothesis* problem it is still meaningful to constrain false alarm probability, the presence of a set of $M-1$ correct detection probabilities as in (4) presents many possibilities for the maximization part of the criterion. What one truly would like to do in the M-hypothesis case is to maximize the *average* correct detection probability (or equivalently minimize the average missed detection probability) subject to a constraint on P_{FA}. in order to

accomplish this one needs knowledge of the a priori probabilities of the M - 1 signal hypotheses (to allow computation of the average correct detection probability) which is contrary to the basic tenet of the Neyman-Pearson philosophy, namely, to specify a test that is independent of this knowledge. To arrive at a test that is simple and implementable, we shall choose to maximize the sum of the correct detection probabilities of (4) which is tantamount to maximizing the average correct detection probability *assuming equal a priori probabilities for the M-1 signal hypotheses.* Then setting M=2 will result in the well-known two-hypothesis Neyman-Pearson test as mentioned above.

The above criterion can be formulated mathematically using the concept of LaGrange multipliers. For notational simplicity let $p_i(\mathbf{r}) = p\{\mathbf{r}|H_i\}$, $i = 0,1,2,\ldots,M-1$. Then, the Neyman Pearson test becomes:

Choose the M decision regions R_i, $i = 0,1,2,\ldots,M-1$ so as to minimize

$$F = 1 - \sum_{i=1}^{M-1} P_{Di} + \lambda P_{FA} = 1 - \sum_{i=1}^{M-1} \int_{R_i} p_i(\mathbf{r})d\mathbf{r} + \lambda \sum_{i=1}^{M-1} \int_{R_i} p_0(\mathbf{r})d\mathbf{r}$$
$$= 1 - \sum_{i=1}^{M-1} \int_{R_i} (p_i(\mathbf{r}) - \lambda p_0(\mathbf{r}))d\mathbf{r} \qquad (5)$$

where λ is a LaGrange multiplier to be determined. Thus, for a given observation r, we examine all the values of i for which p,(r) - **Ape(r) > ()** and then choose that value of i, say i^* which yields the *largest* of these positive values of **p,(r) -- Ape(r).** Then, r is assigned to the decision region N,., i.e., based on observation of **r, wc** decide in favor of hypothesis }/i.. Since the decision regions are disjoint, then for any particular value of r , the contribution to the integral $\int_{R_i} (p_i(\mathbf{r}) - \lambda p_0(\mathbf{r}))d\mathbf{r}$ comes only from one of the terms in the summation on i, namely i^*. in terms of a likelihood ratio test, the above can be stated as:

If $\frac{p_i(\mathbf{r})}{p_0(\mathbf{r})} > \lambda$, then choose hypothesis H_i, corresponding to $i^* = \max_i \frac{\mathbf{p,(r)}}{p_0(\mathbf{r})}$

Otherwise (i.e., if $\frac{p_i(\mathbf{r})}{p_0(\mathbf{r})} \le \lambda$ for all $i = 1,2,\ldots,M-1$), choose the hypothesis H_0. (6)

In (6), the notation " $\max_i{}^{-1} f(i)$" means "the value of i that maximizes $j'(i)$". The LaGrange multiplier λ (which from the above test turns out to be the decision threshold) is chosen to satisfy the given constraint on false alarm probability which can be determined from

$$P_{FA} = 1 - \int_{R_0} p_0(\mathbf{r})d\mathbf{r} \qquad (7)$$

where $p_0(\mathbf{r})$ is independent of any of the transmitted signals, $s_i(t),\ldots i = 1,2,\ldots,$ M - 1.

signal present, but also decides on the most likely signal when indeed the latter is true. Returning now to the continuous time notation as originally introduced in Eq. (1), the decision rule of (6) becomes

$$\text{If } \frac{p\left(r(t)|H_i\right)}{p\left(r(t)|H_0\right)} > \lambda, \text{ then choose } H_{i^*} \text{ corresponding to } i^* = \max_i{}^{-1} \frac{p\left(r(t)|H_i\right)}{p\left(r(t)|H_0\right)}.$$
$$\text{If } \frac{p\left(r(t)|H_i\right)}{p\left(r(t)|H_0\right)} \le \lambda \text{ for all } i = 1,2,\ldots,M-1, \text{ choose } H_0. \tag{8}$$

For the two-hypothesis case ($M = 2$), Eq. (8) simplifies to

$$\text{If } \Lambda(r(t)) \stackrel{\Delta}{=} \frac{p\left(r(t)|H_1\right)}{p\left(r(t)|H_0\right)} > \lambda, \text{ then choose } H_1. \text{ If } \Lambda(r(t)) \le \lambda, \text{ then choose } H_0 \tag{9}$$

where $\Lambda(r(t))$ is referred to as the *likelihood ratio.*

3.1 Average- and Maximum-Likelihood Receivers Based on the M-Hypothesis Neyman Pearson Test

In [1], average- and maximum-likelihood receivers were derived and presented for a variety of scenarios corresponding to the amount of parameter information, e.g., carrier phase, carrier frequency, etc., available for the signal. In all cases, the results were obtained only for the two-hypothesis case and as such related to the test for the presence or absence of a single signal modeled as a fixed (known) amplitude sinusoid with known frequency and unknown phase over an AWGN channel. As discussed in the introduction of this paper, the spacecraft monitoring problem corresponds to an M-hypothesis (typically M-1 signals and one null hypothesis) test and thus it is of interest to reexamine the structure and performance of the receivers in [1] in light of the additional signal hypotheses.

The evaluation of the numerator of the likelihood ratio $\Lambda(r(t))$ for a signal with unknown parameters requires that one first determine the pdf of the received signal under hypothesis H_1 conditioned on the vector of unknown parameters and then average over the joint pdf of these parameters. Letting $\boldsymbol{\alpha}$ denote this random parameter vector (which as mentioned above would typically include carrier phase, carrier frequency, and the possibly other frequency derivatives), then the likelihood ratio is computed from

$$\Lambda(r(t)) = \frac{\int_{\alpha} p\left(r(t)|H_1,\boldsymbol{\alpha}\right)p(\boldsymbol{\alpha})d\boldsymbol{\alpha}}{p\left(r(t)|H_0\right)} \tag{10}$$

This is referred to as the *average-likelihood ratio (ALR) approach* and is optimum in the context of the Neyman-Pearson criterion previously discussed. Ordinarily, the unknown random parameters are independent random variables and thus the joint

unknown random parameters are independent random variables and thus the joint pdf $p(\alpha)$ becomes a product of the individual pdfs characterizing each parameter and hence the multidimensional integral in (10) becomes a product of integrals.

An alternate approach is to compute the numerator of the likelihood function by again first determining the pdf of the received signal under hypothesis H_1 conditioned on the vector of unknown parameters, but then replacing the random parameters with suitable estimates of these parameters rather than averaging over their joint pdf. One such set of estimates is the maximum-likelihood (ML) estimates and leads to the *maximum-likelihood ratio (MLR) approach* which is mathematically characterized by

$$\hat{\Lambda}(r(t)) = \frac{p\left(r(t)|H_1, \hat{\alpha}_{ML}\right)}{p\left(r(t)|H_0\right)} \tag{11}$$

where $\hat{\alpha}_{ML}$ is the ML estimate of the parameter vector α. Note that under no circumstances is $\hat{\Lambda}(r(t))$ ever equal to $\Lambda(r(t))$ and except in some very specialized cases (he' AI.R and the Ml .R philosophies do not result in the same likelihood-ratio (LR) *test*. One case where they do result in the same 1 .R test (as pointed out in [1]) occurs for a signal which is an unmodulated sinusoidal tone (carrier) all of whose parameters are known except for its phase which is assumed to be uniformly distributed in the interval $(-\pi, \pi)$.

in a more general context, structures derived from replacing the unknown parameters in the pdf of the received signal under hypothesis H_1 conditioned on the vector of unknown parameters with estimates of them are referred to as *estimat - correlator* structures. The reason for this is that the form of these structures involves a correlation of the received signal plus noise, $r(t)$, with a suitable estimate of the transmitted signal followed by comparison with a threshold determined from the specified false alarm probability. in fact, it was shown almost three decades ago by Kailath [2] that receiver structures derived from an AI.R test *always* have an equivalent formulation (leading to an equivalent likelihood ratio test) in terms of an estimator-correlator structure provided that *the appropriate signal estimator is used*.[2] in this context, it was shown that the correct signal estimator to use in the est imator-correl ator structure is the *minimum mean-square est imator (MMSE) based on observation of* the *received signal* 14p *to the present time.* Since the MMSE estimator of the signal up to the present time is not equal to the signal estimate obtained using ML estimates of the signal parameters obtained from the full observation interval, it is unlikely that the two will yield equivalent likelihood ratio tests. Equivalently, the Al .R (which is equivalent to the estimator-correlator with the MMSE signs

[2]Note that Kailath refers to what we call an *average-likelihood ratio* test as a *generalized likelihood ratio* test.

different performances. As mentioned above, only in very special cases will the ALR and MLR approaches result in equivalent LR tests. Thus, in most circumstances, *estimator-correlator receivers using the ML parameter estimates to arrive at the signal estimator, i.e., the MLR approach, will result in suboptimum performance relative to the ALR approach.*

3.1.1 ALR and MLR Structures

In generalizing the ALR and MLR two-hypothesis receivers to M hypothesis structures, we observe from (8) that the optimum test still involves comparison of a likelihood ratio $\Lambda_i(r(t)) \triangleq p(r(t)|H_i)/\ p(r(t)|H_0)$ (which now depends on which signal hypothesis is being considered) with a threshold. The specific structure of these receivers depends on the form of the *M-1* signals representing the signal plus noise hypotheses. in line with the signal form assumed in [1], namely, a fixed amplitude sinusoid with either unknown phase and known frequency or both unknown phase and unknown frequency, we shall assume for the M-hypothesis case a set of *M-1* sinusoids (at frequencies $f_{c,1}, f_{c,2}, \ldots, f_{c,M-}$,) with the same unknown parameters. 'J'bus, the set of signals in (1) is mathematically modeled by

$$s_i(t) = \sqrt{2P}\cos(2\pi f_{ci}t + 0), \quad i = 1,2,\ldots, M - 1 \tag{12}$$

where P, f_{ci} respectively denote the known signal power and radian carrier frequency of the ith signal and 0 denotes the uknown carrier phase assumed to be uniformly distributed in the interval $(-\pi, \pi)$. Since the best performance with such a signaling set is achieved when the signals are equal energy and *orthogonal*, we shall make this further assumption here. Note, however, that the *structure* of the optimum ALR and MLR receivers does not require this orthogonality constraint. Without going into great detail we briefly summarize here the results for the specific cases treated in [1]. The reader is referred to [1] for more detail on the two-hypothesis case.

a. Sinusoidal Carriers with Unknown Phase and Known Frequency - ALR, MLR

The optimum ALR or MLR receiver computes for each of the *M-1* transmitted frequencies the envelope

$$I_i = \sqrt{I_{ci}^2 + I_{si}^2}, \qquad I_{ci} \triangleq \int_0^T r(t)\sqrt{2}\cos 2\pi f_{ci}t\, dt, \quad I_{si} \triangleq \int_0^T r(t)\sqrt{2}\sin 2\pi f_{ci}t\, dt, \quad i = 1,2,\ldots,M-1 \tag{13}$$

The decision rule in both cases is:

If $I_i^2 > \gamma$ for any i, *choose* hypothesis H_i, (or equivalently $s_i(t)$) corresponding to $\max_i I_i^2$. Otherwise ($I_i^2 \leq \gamma$ for all $i = 1,2,\ldots,M-1$) choose hypothesis H_0 (corresponding to no signal sent).

In the MLR case, it is understood that the unknown carrier phase is to be replaced by its ML estimate for *each* of the conditional likelihood ratios so that the decision rule is determined from a comparison of the set $\hat{\Lambda}_i(r(t)) = p\left(r(t)\middle|H_i,\hat{\theta}_{iML}\right)/p\left(r(t)\middle|H_0\right)$, $i = 1,2,\ldots M-1$ with a threshold. Note that the ML phase estimate now depends on the hypothesis H_i. A receiver that implements the above decision rule is illustrated in Fig. 1.

b. Sinusoidal Carriers with Unknown Phase and Unknown Frequency - ALR

Assuming a frequency uncertainty region of $\pm B/2$ Hz around each of the possible transmitted tones, then the optimum ALR receiver computes for each of the M-1 transmitted frequencies the quantity[3]

$$Y_i \triangleq \int_{f_{ci}-B/2}^{f_{ci}+B/2} I_0\left(\frac{2\sqrt{P}}{N_0} L(f)\right) df, \quad i = 1,2,\ldots,M-1 \tag{14}$$

where $L(f)$ s defined analogous to (13) by

$$L(f) = \sqrt{I_c^2(f)+I_s^2(f)}, \qquad I_c(f) \triangleq \int_0^T r(t)\sqrt{2}\cos 2\pi f t\, dt, \quad I_s(f) \triangleq \int_0^T r(t)\sqrt{2}\sin 2\pi f t\, dt \tag{15}$$

The decision rule is:

> If $Y_i > \gamma$ for any i, choose hypothesis H_i (or equivalent] y $s_i(t)$) corresponding to $\max_i Y_i$. Otherwise (1($\leq \gamma$ for all i = 1,2,.,., M - 1) choose hypothesis H_0 (corresponding to no signal sent).

Since (14) is overly demanding to implement, one discretizes each of the M-1 frequency uncertainly intervals into $G = B/T^{-1} = BT$ subintervals to each of which is dissociated a candidate frequency $f_{ci,j}, i = 1,2,\ldots,M-1, j = 0,1,\ldots,G$ --1 located at its center. Such a discretization results in orthogonal envelope detector outputs. As such, the integration over the continuous uncertainty regions in (14) is approximate'd by a discrete (Riemann) sum and, hence, the approximate statistic to be used in the decision rule is

$$Y_i \cong \sum_{j=0}^{G-1} I_0\left(\frac{2\sqrt{P}}{N_0} L(f_{ci,j})\right), \qquad i = 1,2,\ldots, M-1 \tag{16}$$

A receiver that implements the above decision rule is illustrated in Fig. 2.

c. Sinusoidal Carriers with Unknown Phase and Unknown Frequency - MLR

Again assuming disjoint frequency uncertainty regions of $\pm B/2$ Hz around each of the possible transmitted tones, then the' optimum ML R receiver computes for each of the *M-1* transmitted frequencies the quantity

[3] We further assume that the nominal carrier frequencies Of the tones are chosen sufficiently far apart so that the frequency uncertaintly bands around each are nonoverlapping.

$$Y_i = \max_f L(f), \quad f_{ci} - B/2 \le f \le f_{ci} + B/2 \tag{17}$$

where $L(f)$ is defined in (15). The decision rule is the same as that following Eq. (15) and results in a *spectral maximum* form of receiver. Again because of the excessive demand placed on the implementation by the need 10 evaluate (1 7) over a continuum of frequencies, we again quantize each of the frequency uncertainty regions into $G = BT$ subintervals, each with an associate candidate frequency $f_{ci,j}$, $i = 1,2,\ldots,M$ - 1, $j = 0,1,\ldots,G$ - 1 located at its center. As such, the frequency continuous test statistic of (1 7) can be approximated by the discrete form

$$Y_i = \max_j L(f_{ci,j}) \tag{18}$$

A receiver that implements the above decision rule is illustrated in Fig. 3.

3.1.2 Performance of the Al R and MLR Structures

The detection performance of the frequency discrete Al R receiver in Fig. 2 cannot be obtained in closed form due to its highly complex nonlinear structure. Despite its complexity, however, it is important 10 obtain the performance of this receiver since it serves as a benchmark against which the performance of any other simpler to implement structures (including those derived from MI R theory) can be compared. '1'bus, to obtain this performance we shall resort to results obtained from computer simulations. in constructing the simulation for the signal plus noise hypotheses, a decision must be made regarding the selection of the true received frequency of the input signal. in making this selection it is important to understand that spacing the frequencies $f_{ci,j}, j = 0,1,2,\ldots,G$ - 1 for each of the signal hypotheses $H_i, i = 1,2,\ldots,h4$ --1 by $1/T$ guarantees independence of the noise components that appear at the output of each the spectral estimate channels. 1 lowever, orthogonality of the signal components of these same outputs depends on the true value of the received frequency relative to the discretized frequencies assumed for implementation of the receiver. That is, if the true received frequency happens to fall on one of the $f_{ci,j}$'s, then a signal component will appear only in the corresponding spectral estimate channel, i.e., all other channels will contains noise only. On the other hand, if the true received frequency falls somewhere between two of the $f_{ci\,j}$'s, then we have 10ss of orthogonality in that a spillover of signal energy occurs in the neighboring spectral estimates. The worst-case spillover would occur when the true received frequency is midway between two of the $f_{ci,j}$'s. (If an FFT implementation is used, then the worst case degradation can be ameliorated by zero padding to interpolate between the frequency samples.) in view of the above, we shall present both best case and worst case performance results corresponding, respectively, to selecting the true received frequency for the simulation identical to one of the $f_{ci\,j}$'s and midway between two of the $f_{ci,j}$'s.

Figure 4 is a plot of miss probability $P_M = 1 - P_D$ versus P/N_0 in dB-Hz for an observation time T = 1000 see, a frequency uncertainty region $\pm$ ii/2 = $\pm$ 1000 I Iz (thus "' $BT = 2 \times 10^6$), a false alarm probability $P_{FA} = 2 \times 10^{-4}$, and M = 5 (four signal plue noise states representing specific spacecraft conditions and one noise only state representing spacecraft failure).[4] These values have been suggested as being typical of the spacecraft monitoring application. Also shown in this figure are the corresponding results for the MLR receiver of Fig. 3 which can be obtained from a straight tforward generalization of the analytical results in [11 to the case $M > 2$. We observe from a comparison of the Al .R and MLR results that the latter is inferior to the former by a P/N_0 amount on the order of 1 dB-Hz for either the best or worst case situation. in each case, the difference between best and worst performance is about 2 dB-Hz.

3.1.4 Low SNR Approximation of the Al .R Structure

With reference to Eq. (16), we observe that to implement the optimum Al .R structure derived from the assumptions of unknown carrier phase and unknown carrier frequency (uncertainly about the nominal carrier), one must build a receiver containing G envelope' detectors and Bessel function nonlinearities. Although theoretically possible, the complexity of such a receiver for the spacecraft monitoring application where the frequency uncertainty interval, B, is on the order of 2 k} Iz and the observation time interval, "f', is on the order of 1000 see, yielding G = BT = 2 x 106 is simply too great. As such, we seek an alternate approach which combines this large bank of noncoherent processors into perhaps a single noncoherent processor thus greatly reducing the implementation burden.

One such approach is obtained by approximating the $I_0(x)$ Bessel function by its small argument equivalent. in particular, for small values of x, we have $I_0(x) \approx 1 + (0.25x^2$. Of course one could simply make this approximation for the Bessel functions in the discrete frequency form of the decision statistic as given by (16) which would suggest the low SNR Al .R receiver of Fig. 5 (also see Fig. 7-11 of [4]). While this approach is useful in computing the approximate detection performance of the receiver (as we shall see shortly), unfortunately it only reduces the complexity per channel (by eliminating the need for the square root and Bessel function nonlinearities) but does not reduce the complexity in terms of the number of parallel channels needed. On the other hand, making the above Bessel function approximation in the continuous frequency form of the decision statistic as given by (14) together with (1 .5) results in

[4] These parameters arc typical of a spacecraft monitoring system currently under consideration by the Jet Propulsion 1 aboratory for future deep space missions.

$$Y_i \approx \int_{f_{ci}-B/2}^{f_{ci}+B/2}\left[1+\frac{P}{N_0^2}\left(I_c^2(f)+I_s^2(f)\right)\right]df$$

$$= B+\frac{P}{N_0^2}\int_{f_{ci}-B/2}^{f_{ci}+B/2}\left(I_c^2(f)+I_s^2(f)\right)df,\quad i=1,2,\ldots,M-1$$

Substituting for $I_c^2(f)$ and $I_s^2(f)$ from (15) gives

$$Y_i \approx B+\frac{2P}{N_0^2}\int_{f_{ci}-B/2}^{f_{ci}+B/2}\int_0^T\int_0^T r(t)r(\tau)\cos 2\pi ft\cos 2\pi f\tau\,dt\,d\tau\,df$$

$$+\frac{2P}{N_0^2}\int_{f_{ci}-B/2}^{f_{ci}+B/2}\int_0^T\int_0^T r(t)r(\tau)\sin 2\pi ft\sin 2\pi f\tau\,dt\,d\tau\,df \qquad (20)$$

$$= B+\frac{2P}{N_0^2}\int_0^T\int_0^T r(t)r(\tau)\left(\int_{f_{ci}-B/2}^{f_{ci}+B/2}\cos 2\pi f(t-\tau)df\right)dt\,d\tau$$

Shifting the integration on f to the interval $(-B/2,B/2)$, and then performing this integration, (20) evaluates to

$$Y_i \approx B+\frac{P}{N_0^2}\int_0^T\int_0^T r(t)r(\tau)\cos 2\pi f_{ci}(t-\tau)\frac{B\sin\left[\pi B(t-\tau)\right]}{\pi B(t-\tau)}dt\,d\tau$$

$$= B+\frac{P}{N_0^2}\int_0^T r(t)\cos 2\pi f_{ci}t\left(\int_0^T r(\tau)\cos 2\pi f_{ci}\tau\frac{B\sin\left[\pi B(t-\tau)\right]}{\pi B(t-\tau)}d\tau\right)dt \qquad (21)$$

$$+\frac{P}{N_0^2}\int_0^T r(t)\sin 2\pi f_{ci}t\left(\int_0^T r(\tau)\sin 2\pi f_{ci}\tau\frac{B\sin\left[\pi B(t-\tau)\right]}{\pi B(t-\tau)}d\tau\right)dt$$

For $B>>1/T$, i.e., large BT product, as is the case of interest here, we can interpret the integrals on τ as the output of a unit amplitude rectangular low pass filter of bandwidth B excited by the I and Q demodulated (at frequency f_{ci}) input. Strictly speaking this interpretation is only valid in the limit as $T\to\infty$. Denoting these filtered outputs by $y_c(t)$ and $y_s(t)$, we obtain a simple form for (21), namely,

$$Y_i \approx B+\frac{P}{N_0^2}\left[\int_0^T\left(r(t)\cos 2\pi f_{ci}t\right)y_c(t)dt+\int_0^T\left(r(t)\sin 2\pi f_{ci}t\right)y_s(t)dt\right] \qquad (22)$$

which has the physical interpretation illustrated in Fig. 6a. Note that this implementation has the advantage of replacing for each hypothesis an entire bank of G noncoherent processors with a *single* square-and-integrate processing. Since the wideband noise at the inputs to the rectangular filters in Fig. 6a can be separated into an inband component (one whose energy lies in the interval $(-B/2,B/2)$) and a wide out-of-band component (one whose energy lies outside of $(-B/2,B/2)$), then for $B>>1/T$, in so far as the T-sec I&D outputs are concerned, the product of the filter outputs and the wide! out-of-band components can be ignored relative to the product of the filter outputs and the inband components. As such, another approximate form of (21) is

$$Y_i \cong B + \frac{P}{N_0^2}\left[\int_0^T y_s^2(t)dt + \int_0^T y_c^2(t)dt\right] \tag{23}$$

which has the implementation of Fig. 6b. It should be noted that, for any finite T, (22) will always yield better performance than (23); however, in the limit as $T \to \infty$ the two become equivalent. Since both (22) and (23) are approximations to the true low SNR AI R statistic, (23) is the preferable one to use. Furthermore, as we shall soon see, in so far as detection performance is concerned, the rectangular filters of bandwidth B in Fig. 6b are only consequential in determining the number of independent samples (BT) contained in the observation time interval. That is, the performance will not explicitly depend on B or T individually but rather on the product $G = BT$.

The performance of the low SNR approximation to the AI R illustrated in Fig. 5 (which also applies to the implementations in Fig. 6) can be approximately computed by applying a Gaussian assumption to the Y_i's. in particular, using the small argument approximation to the $I_0(x)$ function in (16), we have that

$$Y_i \cong \sum_{j=0}^{G-1}\left(1 + \frac{P}{N_0^2}\hat{L}(f_{ci,j})\right) \triangleq G + Z_i, \qquad i = 1,2,\ldots M-1 \tag{24}$$

Assuming that the transmitted signal is a sinusoid with random phase and frequency identically equal to one of the quantized frequencies of (24), then the mean and variance of Z_i under signal plus noise hypothesis (H_i) anti noise only hypothesis (H_0) can be shown to be

$$E\{Z_i\} \triangleq \bar{Z} = \begin{cases} \frac{PT}{N_0}\left(\frac{PT}{N_0} + G\right), & H_i \\ \frac{PT}{N_0}G, & H_0 \end{cases}$$

$$\operatorname{var}\{Z_i\} \triangleq \sigma_Z^2 = \begin{cases} \left(\frac{PT}{N_0}\right)^2\left(\frac{2PT}{N_0} + G\right), & H_i \\ \left(\frac{PT}{N_0}\right)^2 G, & H_0 \end{cases} \tag{25}$$

From the decision rule following Eq. (15), the false alarm probability is determined from the probability that all $M-1$ Y_i's are below the threshold γ under H_0. Equivalently, absorbing the constant G in (2.4) into the decision threshold and noting that the Y_i's are independent and for large G can be approximated as Gaussian, then P_{FA} is determined from

$$P_{FA} = 1 - \Pr\{Y_1, Y_2, \ldots, Y_{M-1} \le \gamma | H_0\} = 1 - \left[1 - \frac{1}{2}\operatorname{erfc}\left(\frac{\gamma' - \bar{Z}|_{H_0}}{\sqrt{2}\sigma_Z|_{H_0}}\right)\right]^{M-1} \tag{26}$$

where $\gamma' \triangleq \gamma - G$ and $\bar{Z}|_{H_0}, \sigma_Z|_{H_0}$ are determined from (25). Similarly, since under the signal plus noise hypothesis only one of the Y_i's contains the signal, then the detection probability is given by

$$\begin{aligned} P_D &= \Pr\{Y_i > \gamma; Y_1, Y_2, \ldots Y_{i-1}, Y_{i+1}, \ldots, Y_{M-1} \le Y_i | H_i\} \\ &= \int_{\gamma'}^{\infty} \frac{1}{\sqrt{2\pi\sigma_Z^2|_{H_i}}} \exp\left\{-\frac{\left(Z_i - \bar{Z}|_{H_i}\right)^2}{2\sigma_Z^2|_{H_i}}\right\}\left[1 - \frac{1}{2}\operatorname{erfc}\left(\frac{Z_i - \bar{Z}|_{H_0}}{\sqrt{2}\sigma_Z|_{H_0}}\right)\right]^{M-2} dZ_i \end{aligned} \tag{27}$$

where, in addition to the above, $\bar{Z}|_{H_i}, \sigma_Z|_{H_i}$ are determined from (25). Eliminating the normalized threshold between (26) and (27) and making use of the moments in (25), the ROC for the low SNR ALR receiver is approximately (based on a Gaussian model for the Y_i's) given by

$$\begin{aligned} P_D &= \frac{1}{\sqrt{\pi}} \frac{\sigma_Z|_{H_0}}{\sigma_Z|_{H_i}} \int_{\eta}^{\infty} \exp\left\{-\frac{\left(Y\sqrt{2}\sigma_Z|_{H_0} + \bar{Z}|_{H_0} - \bar{Z}|_{H_i}\right)^2}{2\sigma_Z^2|_{H_i}}\right\}\left[1 - \frac{1}{2}\operatorname{erfc} Y\right]^{M-2} dY \\ &= \frac{1}{\sqrt{\pi}} \sqrt{\frac{G}{2PT/N_0}} \int_{\eta}^{\infty} \exp\left\{-\left(\frac{G}{2PT/N_0 + G}\right)\left(Y - \frac{PT/N_0}{\sqrt{2G}}\right)^2\right\}\left[1 - \frac{1}{2}\operatorname{erfc} Y\right]^{M-2} dY, \\ \eta &\triangleq \operatorname{erfc}^{-1}\left\{2\left[1 - (1 - P_{FA})^{\frac{1}{M-1}}\right]\right\} \end{aligned} \tag{28a}$$

For $G >> PT/N_0$ and $P_{FA} << 1$ (the cases of interest here), (28a) simplifies to

$$\begin{aligned} P_D &= \frac{1}{\sqrt{\pi}} \int_{\eta} \exp\left\{-\left(Y - \frac{PT/N_0}{\sqrt{2G}}\right)^2\right\}\left[1 - \frac{1}{2}\operatorname{erfc} Y\right]^{M-2} dY, \\ \eta &\triangleq \operatorname{erfc}^{-1}\left\{\left(\frac{1}{M-1}\right)2P_{FA}\right\} \end{aligned} \tag{28b}$$

Furthermore for the two hypothesis problem, i.e., M = 2, (28a) simplifies to

$$P_D = \frac{1}{2}\operatorname{erfc}\left[\sqrt{\frac{G}{2PT/N_0}}\left(\operatorname{erfc}^{-1}(2P_{FA}) - \frac{PT/N_0}{\sqrt{2G}}\right)\right] \frac{1}{2}\operatorname{erfc}\left[\operatorname{erfc}^{-1}(2P_{FA}) - \frac{PT}{\sqrt{2G}N_0}\right] \tag{29}$$

Fig. 7 is a plot of miss probability $P_M = 1 - P_D$ as determined from (28) and (29) versus $)'//V_o$ in dB-Hz for the same parameters as in Fig. 4. The performance curves for the full-band receiver were obtained numerically from (28a) and the exact form of (29).

For $M = 2$, these results were verified using a computer simulation and are also illustrated in the figure. Comparing Fig. 7 with the ALR results in Fig. 5, we observe the huge penalty in performance paid for the simplicity of implementation afforded by the low SNR approximation.

3.1.5 ALR and MLR Structures for Sinusoidal Carriers with Unknown Phase, Frequency, and Frequency Rate

Assume now that in addition to the uncertainty in phase and frequency of the transmitted sinusoidal carrier considered in Section 3.1.1, there also exists an uncertainty in frequency rate corresponding to the presence of oscillator drift. If this drift is modeled as a linear variation in frequency over the observation interval, i.e., a constant but unknown frequency rate uniformly distributed in the interval $\pm \dot{B}/2$, then following the ALR approach, it is straightforward to show that analogous to (14) the optimum receiver computes for each of the *M-1* transmitted frequencies the quantity

$$Y_i \triangleq \int_{-\dot{B}/2}^{\dot{B}/2} \int_{f_{ci}-B/2}^{f_{ci}+B/2} I_0\left(\frac{2\sqrt{P}}{N_0} L(f,\dot{f})\right) df d\dot{f}, \qquad i = 1,2,\ldots,M-1 \tag{30}$$

where

$$\begin{aligned} L(f,\dot{f}) &= \sqrt{I_c^2(f,\dot{f}) + I_s^2(f,\dot{f})}, \\ I_c(f,\dot{f}) &\triangleq \int_0^T r(t)\sqrt{2}\cos\left[2\pi\left(ft + \tfrac{1}{2}\dot{f}t^2\right)\right]dt \\ I_s(f,\dot{f}) &\triangleq \int_0^T r(t)\sqrt{2}\sin\left[2\pi\left(ft + \tfrac{1}{2}\dot{f}t^2\right)\right]dt \end{aligned} \tag{31}$$

The decision rule is still the same as that following Eq. (15). Since (30) is even more overly demanding to implement than was (14) because of the additional integration on $\dot{f}$, then once again we must resort to discretization of the frequency and frequency rate uncertainty intervals resulting in the approximate decision variables

$$Y_i \triangleq \sum_{j=0}^{G-1} \sum_{l=0}^{F-1} I_0\left(\frac{2\sqrt{P}}{N_0} L(f_{ci,j}, \dot{f}_l)\right), \quad i = 1,2,\ldots, M-1 \tag{32}$$

where $F \triangleq \dot{B}T^2/2.5$ An illustration of an ALR receiver that employs this decision statistic is illustrated in Fig. 8.

In the: presence of linear frequency drift, the optimum MLR receiver would compute for each of the *M-1* transmitted frequencies the quantity

$$Y_i = \max_{f,\dot{f}} L(f,\dot{f}), \; f_{ci} - B/2 \le f \le f_{ci} + B/2, \; -\dot{B}/2 \le \dot{f} \le \dot{B}/2, \tag{33}$$

and then apply the decision rule following Eq. (15). in discretized form, (33) would become (analogous to (18))

[5]The value of F, i.e., the quantization of the $\dot{f}$ uncertainty, is determined from approximate orthogonality considerations (see Appendix C of [8]).

$$Y_i = \max_{j,l} L(f_{ci,j}, \dot{f}_l) \tag{34}$$

3.1.6. Low SNR Approximation of the ALR Stucture

As in Section 3.1.4, one can approximate the zero order modified Bessel function in (32) by the first two terms in its power series. When this is done, then using (31) it is straightforward to show that analogous to (21) one obtains

$$Y_i \equiv B\dot{B} + \frac{P}{N_0^2}\int_0^T r(t)\cos 2\pi f_{ci}t\left(\int_0^T r(\tau)\cos 2\pi f_{ci}\tau \frac{B\sin[\pi B(t-\tau)]}{\pi B(t-\tau)} \frac{\dot{B}\sin\left[\frac{\pi\dot{B}}{2}(t^2-\tau^2)\right]}{\frac{\pi\dot{B}}{2}(t^2-\tau^2)}d\tau\right)dt$$

$$+\frac{P}{N_0^2}\int_0^T r(t)\sin 2\pi f_{ci}t\left(\int_0^T r(\tau)\sin 2\pi f_{ci}\tau \frac{B\sin[\pi B(t-\tau)]}{\pi B(t-\tau)} \frac{\dot{B}\sin\left[\frac{\pi\dot{B}}{2}(t^2-\tau^2)\right]}{\frac{\pi\dot{B}}{2}(t^2-\tau^2)}d\tau\right)dt \tag{35}$$

Unfortunately, (35) does not lend itself to an easy interpretation in terms of an implementation. However, if $(\dot{B}/2)T < B/2$ (i.e., the maximum frequency change due to drift is within the initial baseband frequency uncertainty interval), then over the observation interval the $\sin x/x$ term involving $\dot{B}$ in (35) is much slower varying than the $\sin x/x$ term involving B and to a first order approximation the former can be treated as a constant with respect to the time duration of the latter. As such, the' implementations of Fig. 6a, b are still appropriate for the low SNR approximation to the ALR in the presence of linear frequency drift. Also invoking the Gaussian approximation to the statistics of (35), then to a first order approximation, the detection performance is still given by (28) and (29).

3.1,7. Improved Simple Receiver Structures for Signals with Bounded Frequency Drift

While the square-and-integrate receivers of Fig. 6 have the advantage that their simple structure and performance> are approximately invariant to the presence of frequency drift, as previously mentioned the'y pay a large penalty in performance when compared to the true optimum ALR schemes.[6] in an effort to improve upon this situation, we shall suggest a modification of the simple square-and-

[6]While it is true that the performances of the optimum ALR and MLR structures derived in Sect. 3.1.1 (b), (c) and illustrate in Figs. 2, 3 will degrade in the presence of drift approaching that of the simple receivers of Fig. 6, this will be less true for the optimum ALR and MLR structures derived in the presence of drift as described by the decision statistics in Sect. 3.1.6.

integrate receiver of Fig. 6b by exploiting the fact that, in the case of interest here, $(\dot{B}/2)T << B/2$, i.e., the drift over the observation interval is only a small fraction of the total initial frequency uncertainty band. in particular, typical spacecraft oscillators have a maximum one-sided drift rate on the order of 25 Hz in 1000 seconds and thus for an observation time of 'f' = 1000 sec, $(\dot{B}/2)T = 25$ Hz which is quite small compared to the assumed baseband frequency uncertainty interval of B/2 = 1000117,

Consider dividing the total baseband frequency uncertainty band $B/2$ Hz into K subbands of width $(\dot{B}/2)T$ 117 each, i.e., $K = (B/2)/(\dot{B}/2)T$ which for our ongoing example yields $K = 1000/25 = 40$. A motivation for doing this can be obtained by examining the behavior of the Al .R structure of Fig. 2 when the input frequency drifts and is discussed following the end of this paragraph. The received signal in each of these subbands[7] is squared-and-integrated in the manner of Fig. 6b. The maximum of these squared-and-integrated values (energies) is selected and compared to a threshold set by the requirement on false' alarm probability. A receiver implementation based on M channels of the type described above (see Fig. 9) will be referred to herein as a *subband squaring receiver* as contrasted with a *full band squaring receiver* which would incorporate M channels of the type illustrated in Fig. 6b.

The construction of the subband squaring receiver can be motivated by reexamining, the basic building block of the Al .R receiver in Fig. 2, namely, the envelope detector. in particular, rewriting the squared envelope of the ijth detector as

$$I_{ij}^2(f_{ci,j}) = \left[\int_0^T r(t)\sqrt{2}\cos 2\pi f_{ci,j}t\,dt\right]^2 + \left[\int_0^T r(t)\sqrt{2}\sin 2\pi f_{ci,j}t\,dt\right]^2$$

$$= \left|\int_0^T r(t)\sqrt{2}e^{-j2\pi f_{ci,j}t}\,dt\right|^2 = \left|\int_{-\infty}^{\infty} r(t)p(t)\sqrt{2}e^{-j2\pi f_{ci,j}t}\,dt\right|^2$$

where $p(t)$ is a unit amplitude rectangular pulse in the interval $0 \le t \le T$ shows that $I_{ij}^2(f_{ci,j})$ can be interpreted as the energy component of the windowed signal $r(t)p(t)$ at frequency $f_{ci,j}$ over an effective bandwidth of $1/T$ Hz (the result of frequency domain spreading due to the finite duration of the time window p(t).) Thus, each envelope detector in Fig. 2 measures the energy in a narrow frequency band within the uncertainty band of interest. Since the center frequencies of adjacent envelope detector-s are separated by $1/T$ 1 lz, it is clear that the ith detector in Fig. 2 consists of

[7]From an implementation point of view, the received signal is passed through a bank of disjoint subband bandpass filters each of which can alternately be implemented as an 1-Q demodulation with the carrier frequency at the center of the subband followed by a baseband rectangular filter of width $(\dot{B}/2)T = B/2K$.

a bank of narrowband filters that completely cover the frequency uncertainty region associated with the ith signal. For a square window function, the frequency response of each filter is of the form $\sin x/x$, implying orthogonal outputs when the center frequencies are separated by $1/T$ Hz. Thus, the filter bank generates the maximum number of independent samples, BT, consistent with a bandwidth B Hz, and integration time T sec.

The MLR algorithm selects the largest energy component within the ith filter bank as the test statistic Y_i as illustrated in Fig. 3. For the ALR algorithm, however, the energy components collected at each frequency are further processed by taking the square root, applying a scale factor, and computing the Bessel function $I_0(x)$ of the resulting scaled envelope. Following this, the results are summed to obtain the test statistic Y_i. Although the MLR structure is suboptimum, its performance is only slightly worse than that of the ALR algorithm for this application. Both the ALR and MLR structures are predicated on the assumption that the signal remains constant in frequency, which further implies that it remains within the passband of the same filter (channel) through the entire observation interval, ensuring the greatest possible SNR at the output of that filter. Equivalently, in terms of a changing input frequency, a maximum signal drift of less than $1/T$ Hz over the T-sec observation is implied.

If the maximum frequency drift exceeds $1/T$ Hz during the observation, then the signal moves from one filter to the next, possibly spanning a large number of filters (channels) over the observation interval. In that case, no single filter contains all of the signal energy, which is now distributed among many adjacent filters. However, if the starting frequency and maximum drift rate were known, then the signal energy could still be recovered by combining (summing) the outputs of all filters spanned by the signal. Since the actual starting frequency is not known, this suggests using a filter bank with filter bandwidths large enough to accommodate the drifting signal. Thus, analogous to the ALR approach, we partition the uncertainty region into $K = BT/N$ (N an integer chosen in accordance with the maximum drift rate) filters each of bandwidth N/T Hz, instead of BT filters of bandwidth $1/T$ Hz as was done for the discrete version of the ALR with no frequency drift. The outputs of each subband filter are squared and integrated as shown in Fig. 9. Next, if we were to parallel the development of the ALR structure, we would take the square root of the outputs of each of these larger bandwidth (subband) filters, scale them, compute the Bessel function $I_0(x)$ of the resulting scaled envelopes and sum to obtain the test statistic. We shall consider instead selecting the largest subband filter output within the ith detector as the test statistic for the corresponding ith hypothesis, analogous to what is done in the MLR structure.

For the system parameters of interest the subband squaring receiver achieves

a dramatic performance improvement over the full band squaring receiver primarily due to the reduced noise power in the subbands (each has only $1/K$ of the total noise power) degraded somewhat by occasional errors in selecting the correct subband. Assuming a value of $K = 40$, an illustration of this performance improvement is superimposed on the full band squaring receiver results in Fig. 7. The curve labeled $K = 1$ near the subband performance curves represents the performance of a full-band receiver with uncertainty bandwidth $B = 50117$, and is used to illustrate the small amount of degradation due to choosing among 40 subbands. Note that the additional degradation caused by choosing between five hypotheses instead of two is negligibly small for this case. The subband performance curves were computed using (4 O) and (43) (to be derived shortly), and the two-hypothesis case ($M = 2$) was verified using a computer simulation. Comparing these results with those obtained for the full band receiver, we observe a dramatic improvement in performance which is on the order of 7 dB. The analysis used to obtain these results assumes that the tones start at the boundary between subbands and drift (at no greater rate than their maximum rate) to the boundary of the adjacent subband in either the positive or negative direction from their starting points) As such, the received tone remains Within a given subband over the entire observation interval. The details of the analysis are as follows.

The detection performance of the subband squaring receiver is obtained using a Gaussian approximation analogous to that employed for the full band squaring receiver. in particular, since each of the K subband processors in Fig. 9 is implemented as in Fig. 6b but with low pass rectangular filters that are $1/K$th the bandwidth, then the processor outputs $Y_{ik} \triangleq G/K + Z_{1k}, k = 1,2,\ldots,K$ can be modeled as independent Gaussian random variables with means and variances of Z_{1k} as in (25) but with G replaced by G/K. Assuming first the two hypothesis case, the probability of false alarm, P_{FA}, is equal to the probability that any of the K subband processor outputs exceeds the threshold under H_0. Equivalently, P_{FA} is equal to one minus the probability that none of the subband processor outputs exceed the threshold under H_0 which is the same as one minus the probability that the maximum of the subband processor outputs does not exceed the threshold under H_0. Thus, analogous to (26),

$$P_{FA} = 1 - \Pr\{Y_1 \le \gamma | H_0\} = 1 - \left[1 - \frac{1}{2}\operatorname{erfc}\left(\frac{\gamma''}{\sqrt{2}\,\sigma_Z}\Big|_{H_0}\right)\right]^K \tag{36}$$

where $\gamma'' = \gamma - G/K$ and from the above discussion

$$\bar{Z}\big|_{H_0} = \left(\frac{PT}{N_0}\right)\left(\frac{G}{K}\right)$$
$$\sigma_Z\big|_{H_0} = \left(\frac{PT}{N_0}\right)\sqrt{\frac{G}{K}} \qquad (37)$$

The missed detection probability, P_M, is the probability that the maximum of the subband processor outputs does not exceed the threshold under H_1, which from the above is equivalent to the the probability that none of the subband processor outputs exceed the threshold under H_1. Thus, the correct detection probability, $P_D = 1 - P_M$ is given by

$$P_D = 1 - \Pr\{Y_1 \le \gamma | H_1\}$$
$$= 1 - \left[1 - \frac{1}{2}\operatorname{erfc}\left(\frac{\gamma - \bar{Z}\big|_{H_1}}{\sqrt{2}\sigma_Z\big|_{H_1}}\right)\right]\left[1 - \frac{1}{2}\operatorname{erfc}\left(\frac{\gamma - \bar{Z}\big|_{H_0}}{\sqrt{2}\sigma_Z\big|_{H_0}}\right)\right]^{K-1} \qquad (38)$$

where now

$$\bar{Z}\big|_{H_1} = \left(\frac{PT}{N_0}\right)\left(\frac{PT}{N_0} + \frac{G}{K}\right)$$
$$\sigma_Z\big|_{H_1} = \left(\frac{PT}{N_0}\right)\sqrt{\frac{2PT}{N_0} + \frac{G}{K}} \qquad (39)$$

Note that (38) differs in form from (27) since here a correct detection occurs if *any* of the subband processor outputs exceeds the threshold, not necessarily only the one that contains the signal. In detecting among many hypotheses as in (27), a correct detection only occurs if the particular full band processor output that contains the signal exceeds the threshold. Eliminating the threshold between (36) and (38) and making use of the moments in (37) and (39) gives the two hypothesis ROC as

$$P_D = 1 - \left[1 - P_{FA}\right]^{(K-1)/K} \times \left[1 - \frac{1}{2}\operatorname{erfc}\left\{\sqrt{\frac{G/K}{2PT/N_0 + G/K}}\left(\operatorname{erfc}^{-1}\left(2\left[1 - (1 - P_{FA})^{1/K}\right]\right) - \frac{PT/N_0}{\sqrt{2G/K}}\right)\right\}\right] \qquad (40)$$

For $K = 1$, i.e., the full band squaring receiver, (40) reduces to (29) as it should.

For the M hypothesis case, the probability of false alarm, P_{FA}, is given by

$$P_{FA} = 1 - \Pr\{Y_1, Y_2, \ldots, Y_{M-1} \le \gamma | H_0\} = 1 - \left[1 - \frac{1}{2}\operatorname{erfc}\left(\frac{\gamma - \bar{Z}\big|_{H_0}}{\sqrt{2}\sigma_Z\big|_{H_0}}\right)\right]^{K(M-1)} \qquad (41)$$

where $\bar{Z}_{H_0}$ and $\sigma_Z\big|_{H_0}$ are as defined in (37). Similar to (27), the probability of

detection, P_D, is given by

$$P_D = \Pr\left\{Y_i > \gamma; Y_1, Y_2, \ldots Y_{i-1}, Y_{i+1}, \ldots, Y_{M-1} \le Y_i \middle| H_i\right\} \tag{4?}$$

which, by eliminating the threshold, can be shown to be evaluated in terms of P_{FA} as

$$\begin{aligned} P_D = & \frac{1}{\sqrt{\pi}} \sqrt{\frac{G/K}{2PT/N_0 + G/K}} \int_\eta^\infty \exp\left\{-\left(\frac{G/K}{2PT/N_0 + G/K}\right)\left(Y - \frac{PT/N_0}{\sqrt{2G/K}}\right)^2\right\} \\ & \times\left[1 - \frac{1}{2}\operatorname{erfc} Y\right]^{K(M-2)+K-1} dY \\ & + \frac{K-1}{\sqrt{\pi}} \int_\eta^\infty \exp\left\{-Y^2\right\}\left[1 - \frac{1}{2}\operatorname{erfc}\left\{\sqrt{\frac{G/K}{2PT/N_0 + G/K}}\left(Y - \frac{PT/N_0}{\sqrt{2G/K}}\right)\right\}\right] \\ & \times\left[1 - \frac{1}{2}\operatorname{erfc} Y\right]^{K(M-2)+K-2} dY \end{aligned} \tag{43}$$

$$\eta \triangleq \operatorname{erfc}^{-1}\left\{2\left[1 - \left(1 - P_{FA}\right)^{\frac{1}{K(M-1)}}\right]\right\}$$

For $K = 1$, i.e., the full band squaring receiver, (43) reduces to (28a) as it should.

A further improvement in performance can be obtained by designing a receiver that attempts to remove the linear drift component of the received signal, thus enabling one to significantly reduce the size of the frequency subbands. This process, which shall be referred to as *drift matching* constitutes replacing the correlating signals in Fig. 9 with ones that also contain test values of the linear drift distributed over the range corresponding to its maximum positive and negative values. The resulting *drift-matching squaring receiver* illustrated in Fig. 10 can now be motivated from the Al .R with frequency drift (see Fig. 8) just as the subband squaring receiver was motivated by the structure of the Al .R without drift (see Fig. ?). The key idea here is to select channel bandwidths, i.e., the value of K in the input low pass rectangular filters, wide enough to encompass the signal after a linear drift component has been removed. Thus, the minimum channel bandwidth is ultimately determined by the *residual* quadratic and higher order terms in the frequency trajectory. In contrast to Fig. 9, the subband no longer need include the frequency variation corresponding to the maximum linear frequency drift over the observation interval. This receiver structure is quite similar to the maximum-likelihood estimator of frequency and frequency rate described earlier in [7].

"1'0 obtain the ROC of Fig. 10, we proceed as follows. Letting J denote the number of test values of $\dot{f}$ per test value of f, then the false alarm and detection probabilities are given by (36) and (38) respectively with K replaced by KJ. The moments of the decision variables under the noise only and signal plus noise hypotheses are still given by (37) and (39), respectively, keeping in mind, however, that the value of K to be used in these equations is significantly larger than that

previously used for the subband receiver of Fig. 9. Finally, eliminating the unknown detection threshold between (36) and (38) results in the following ROC for the two hypothesis case:

$$P_D = 1 - \left[1 - P_{FA}\right]^{(KJ-1)/KJ} \times \left\{ 1 - \frac{1}{2}\,\mathrm{erfc}\left[\sqrt{\frac{G/K}{2PT/N_0 + G/K}}\left(\mathrm{erfc}^{-1}\left(2\left[1 - (1 - P_{FA})^{1/K}\right]\right) - \frac{PT/N_0}{\sqrt{2G/K}}\right)\right]\right\} \quad (44)$$

For $J = 1$, (44) reduces to (40) as it should.

For the M hypothesis case, the probability of false alarm is once again given by (41) with K replaced by KJ and the probability of detection is still given by (42). Eliminating the threshold between the two probabilities gives an ROC analogous to (43), namely,

$$\begin{aligned} P_D = {} & \frac{1}{\sqrt{\pi}}\sqrt{\frac{G/K}{2PT/N_0 + G/K}}\int_\eta^\infty \exp\left\{-\left(\frac{G/K}{2PT/N_0 + G/K}\right)\left(Y - \frac{PT/N_0}{\sqrt{2G/K}}\right)^2\right\} \\ & \times\left[1 - \frac{1}{2}\,\mathrm{erfc}\,Y\right]^{KJ(M-2)+KJ-1} dY \\ & + \frac{KJ-1}{\sqrt{\pi}}\int_\eta^\infty \exp\{-Y^2\}\left[1 - \frac{1}{2}\,\mathrm{erfc}\left[\sqrt{\frac{G/K}{2PT/N_0 + G/K}}\left(Y - \frac{PT/N_0}{\sqrt{2G/K}}\right)\right]\right] \quad (45) \\ & \times\left[1 - \frac{1}{2}\,\mathrm{erfc}\,Y\right]^{KJ(M-2)+KJ-2} dY \end{aligned}$$

$$\eta = \mathrm{erfc}^{-1}\left\{2\left[1 - (1 - P_{FA})^{\frac{1}{KJ(M-1)}}\right]\right\}$$

The performance of the receiver in Fig. 10 as described by (44) and (45) is superimposed on the results of Fig. 7. Values of (K, J) corresponding to (500, 25), (1 000, 50) and (2000, 1 00) were assumed 10 characterize the performance of the drift-matching subband squaring receiver. Difficulties in computing the large number of test statistics required for this structure prevented verification by means of computer simulations. Note that J is determined from the maximum total (positive and negative) drift $\dot{B}T$, the maximum total (positive and negative) frequency uncertainty B, and K by $J = 2K\dot{B}T/B$ where we have assumed that the subbands of width Ii/K within the total drift $\dot{B}T$ overlap by $B/2K$. Comparing these results with those obtained for the subband receiver of Fig. 9, we see another dramatic improvement in performance. As before, performance for $M = 5$ (four signals) is only slightly worse than for $M = 2$ (the single tone case).

References

[1] M. K. Simon, M. M. Shihabi, and T. Moon, "Optimum detection of tones transmitted by a spacecraft," TDA Progress Report 42-123, November 15, 1995.

[2] T. Kailath, "General likelihood-ratio formula for random signals in Gaussian noise," *IEEE Transactions on Information Theory*, vol. IT-15, no. 3, May 1969, pp. 350-361.

[3] W. C. Lindsey and M.K. Simon, *Telecommunication Systems Engineering*, Prentice-Hall, Inc., Englewood Cliffs, NJ, 1973. Reprinted by Dover Press, New York, NY, 1994.

[4] A. D. Whalen, *Detection of Signals in Noise*, Academic Press, NY, 1971.

[5] H. L. VanTrees, *Detection, Estimation, and Modulation Theoy, Part III*, John Wiley & Sons, New York, NY, 1968, pp. 46-49.

[6] M. Abramowitz and I. A. Stegun, *Handbook of Mathematical Functions*, National Bureau of Standards Applied Mathematics Series 55, U.S. Dept. of Commerce, 1964.

[7] V. A. Vilnrotter, S. Hinedi and R. Kumar, "Frequency Estimation Techniques for High Dynamic Trajectories," *IEEE Transactions on Aerospace and Electronic Systems*, vol. 25, no. 4, July 1989, pp. 559-577.

[8] M. K. Simon, V. Vilnrotter, A. Mileant, S. Hinedi, *Optimum Strategies for Monitoring the Operation Status of a Spacecraft*, to appear in TDA Progress Report 42-127, Jet Propulsion Laboratory, Pasadena, CA.

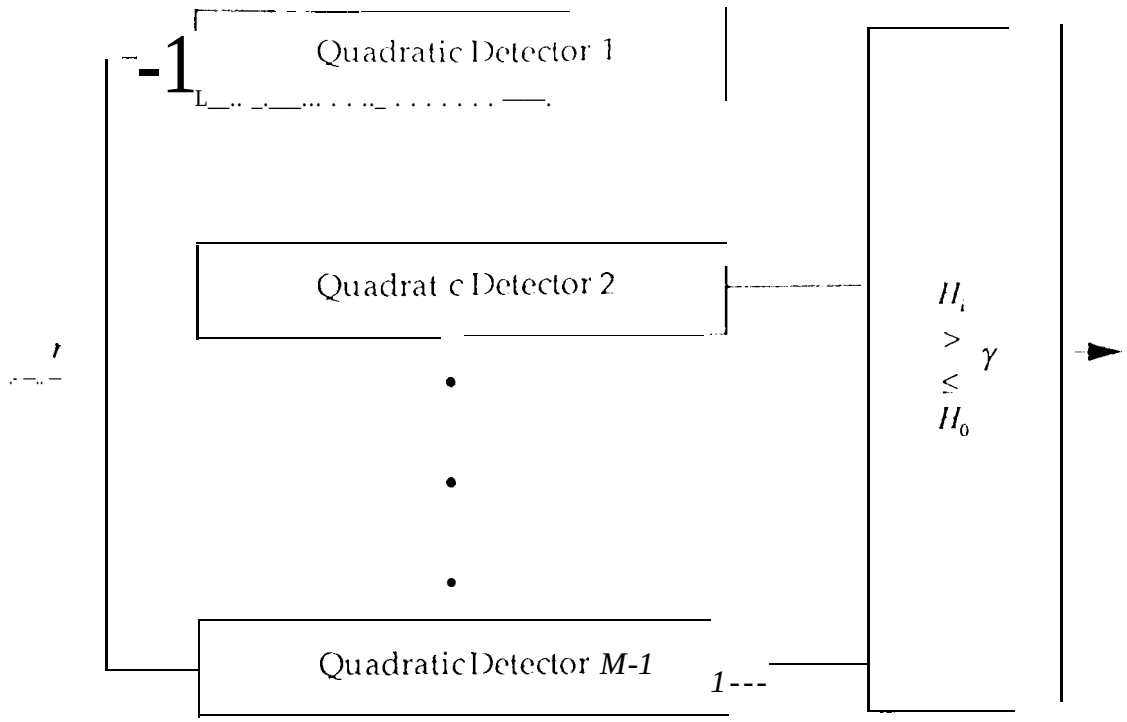

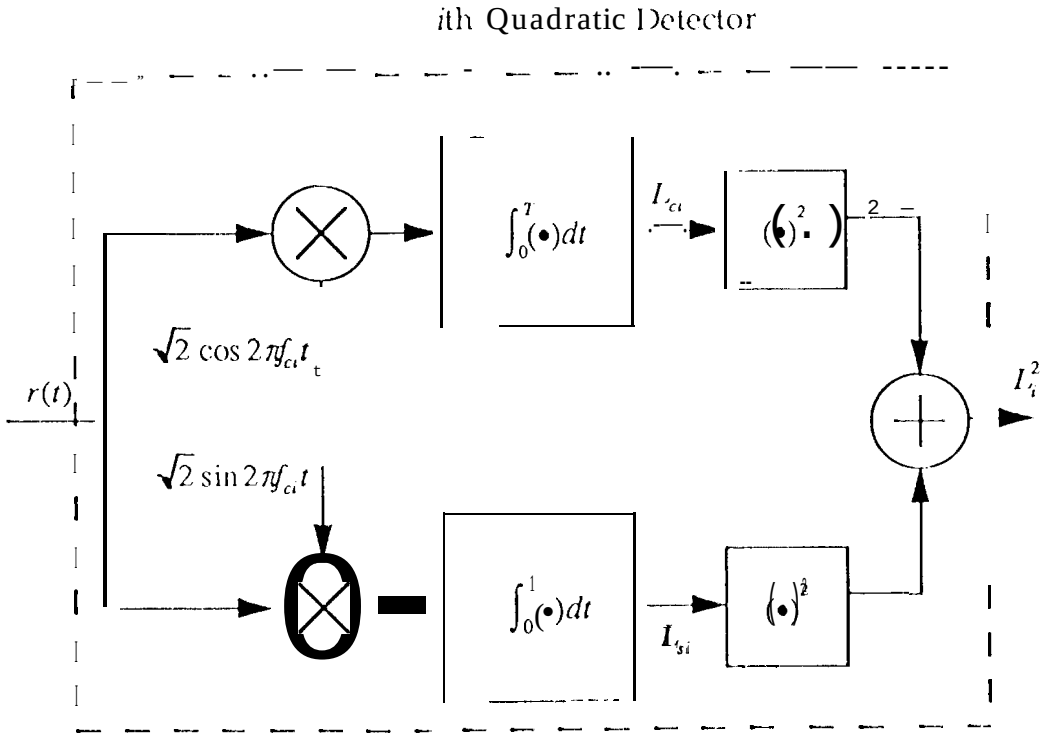

Fig. 1. Average-l,ikelil~[Jod Ratio (ALR) Detector of M-1 Sinusoidal Tones with Known Frequency and Unknown l'base in AW GN

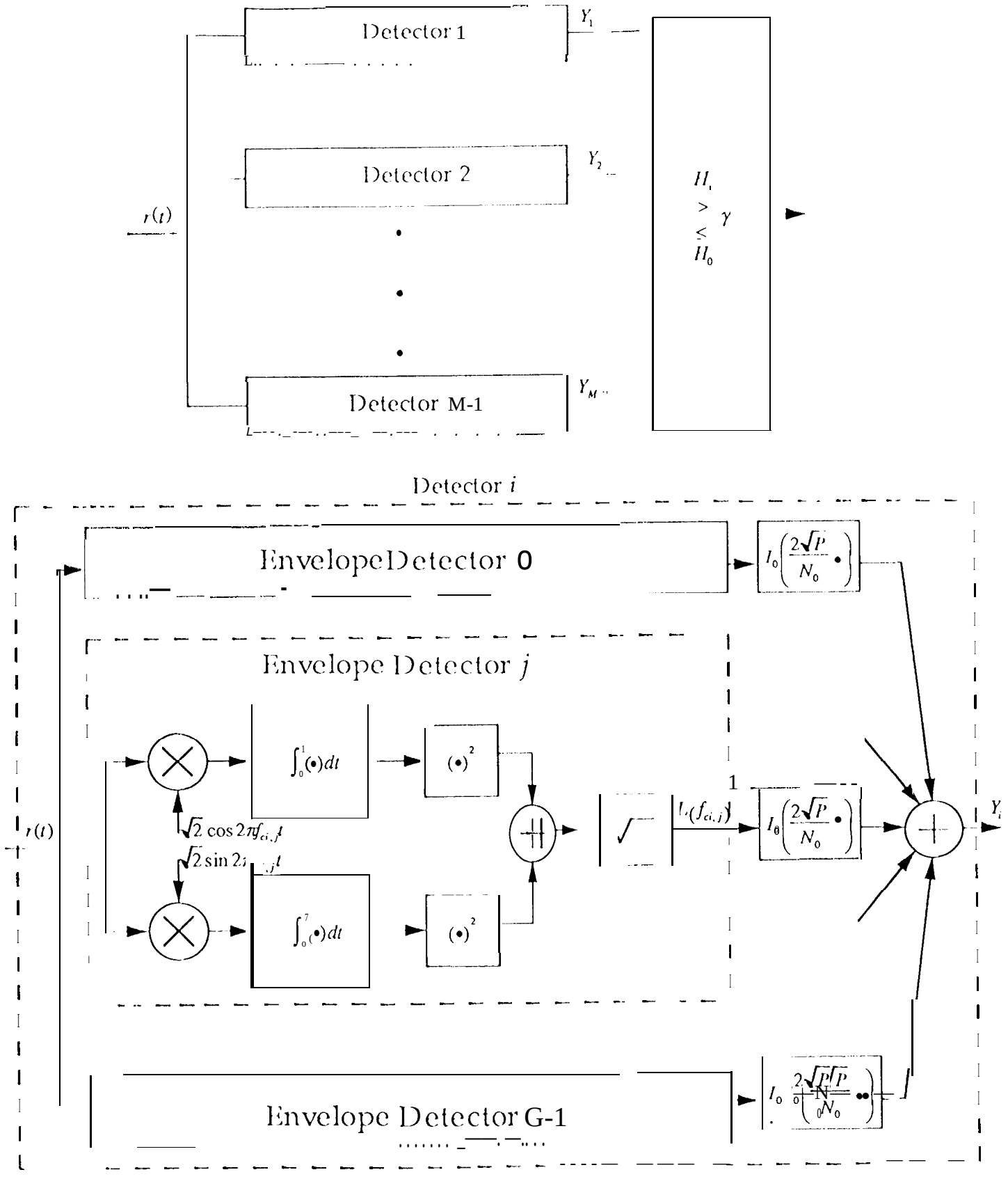

Fig. 2. ALR Detection of M-1 Sinusoidal Tones with Unknown Frequency and Unknown Phase in AWGN

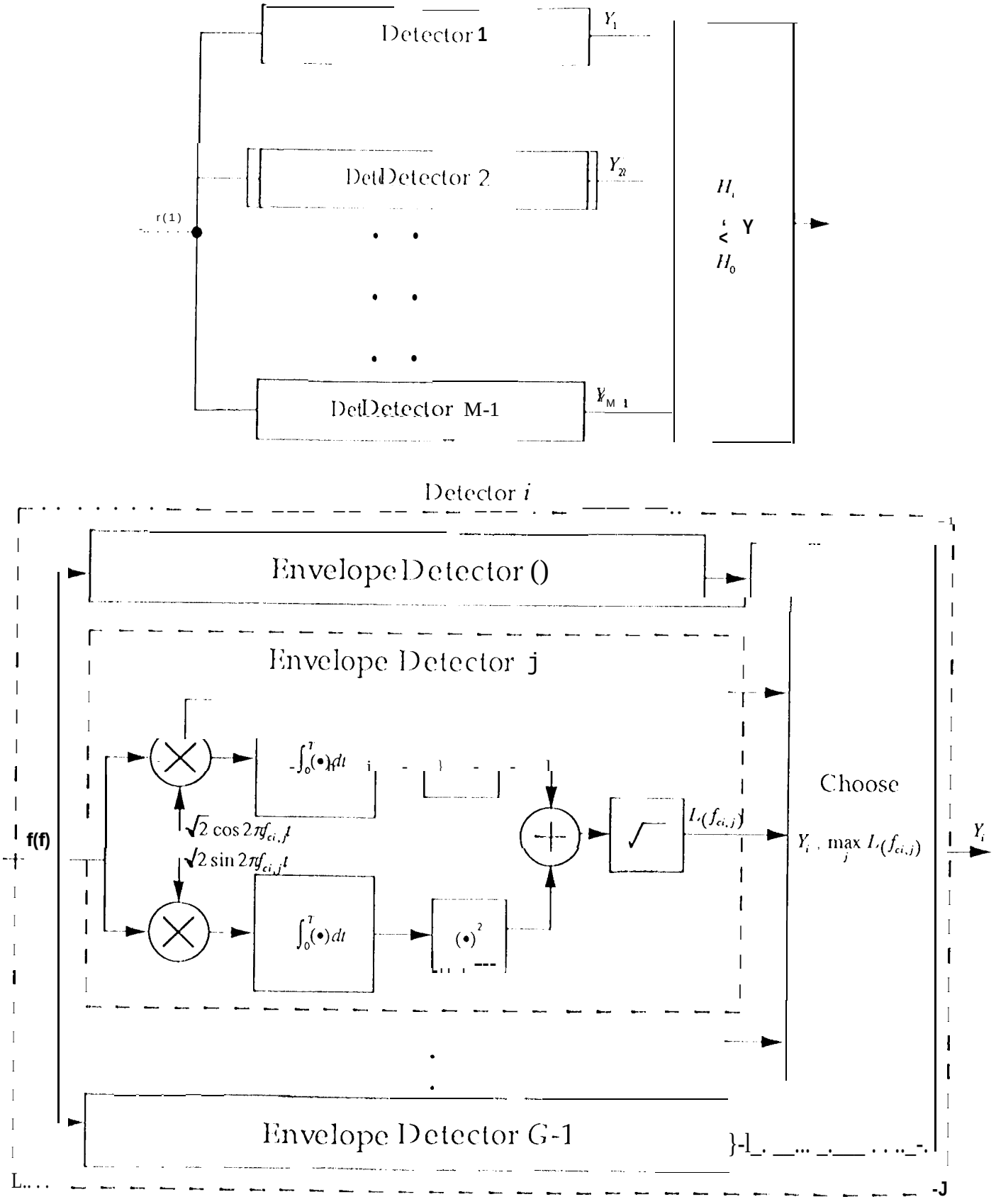

Fig. 3. Maximum-Likelihood Ratio (Ml,]<) Detection of M-1 Sinusoidal Tones with Unknown Frequency and Unknown Phase in AWG N

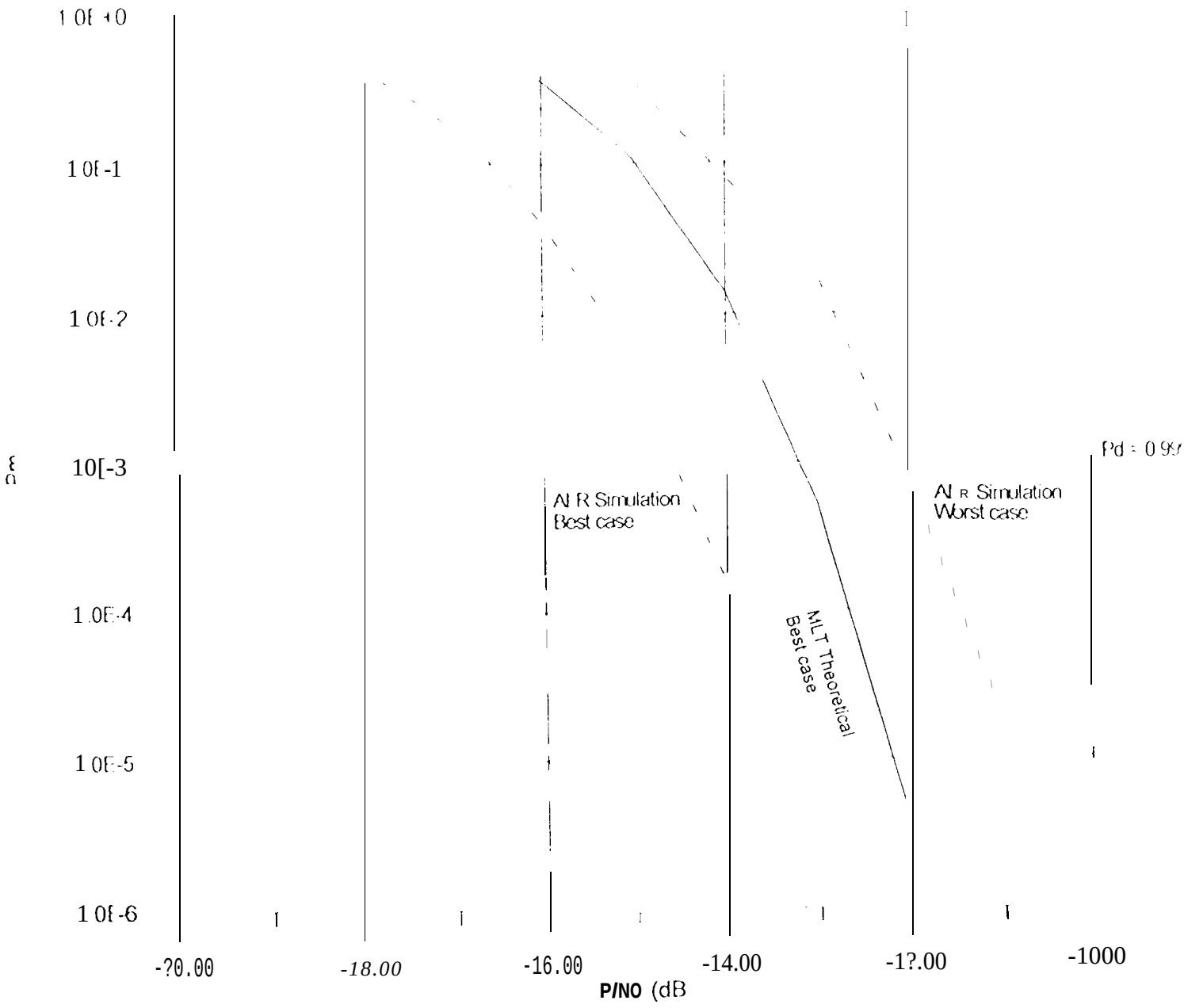

Figure4. Probability of miss, Pm, vs P/NO. at Pf=0.0002
MLR Theory (best case), ALR Simulation (Best and Worst cases)
B=2000Hz, T=1000sec, (N=2*10^6), M = 60000

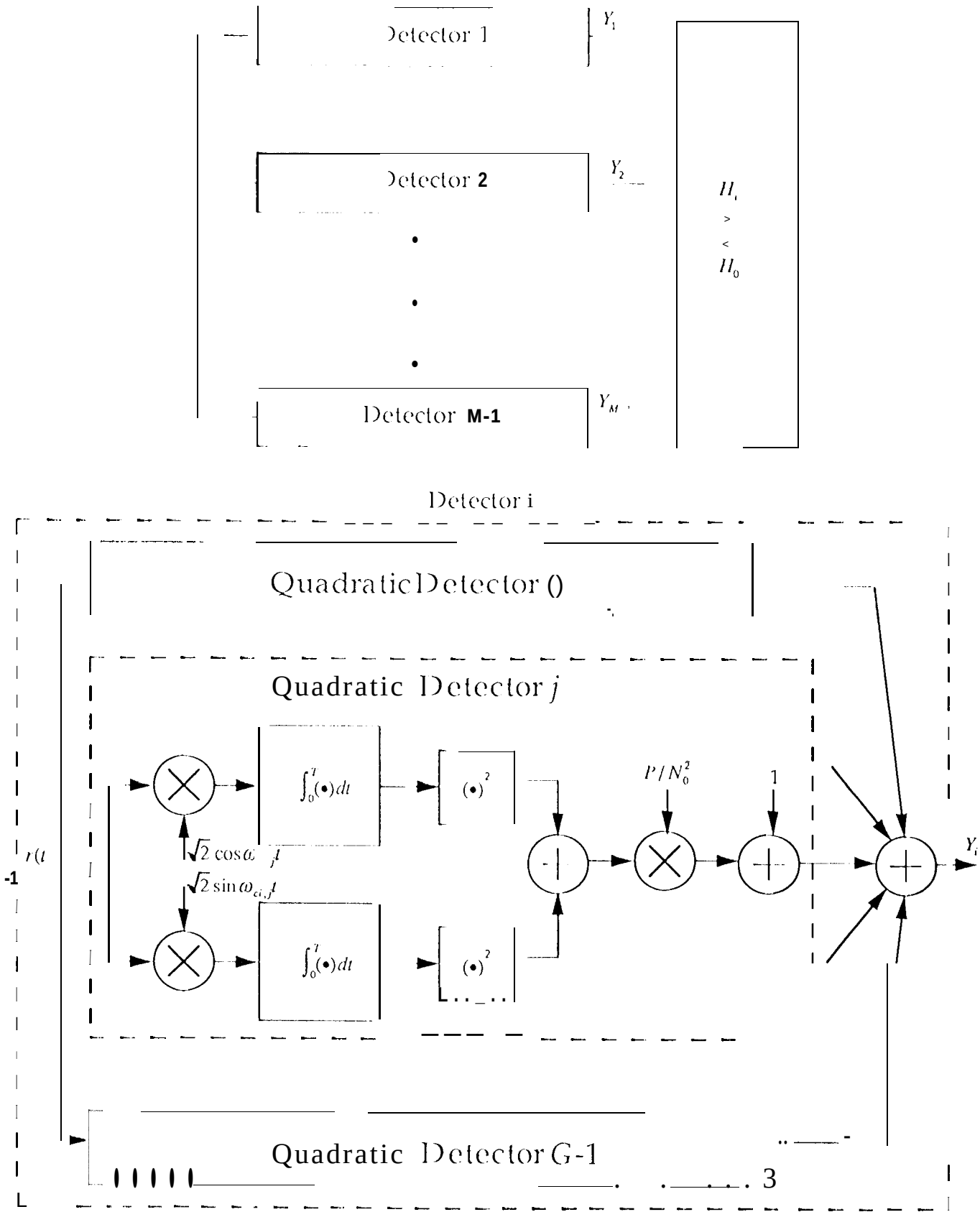

Fig. 5. Low SNR Approximation to the Al .R Detection of *M-1* Sinusoidal Tones with Unknown 1 Frequency and Unknown 1 'ha se in AWG N

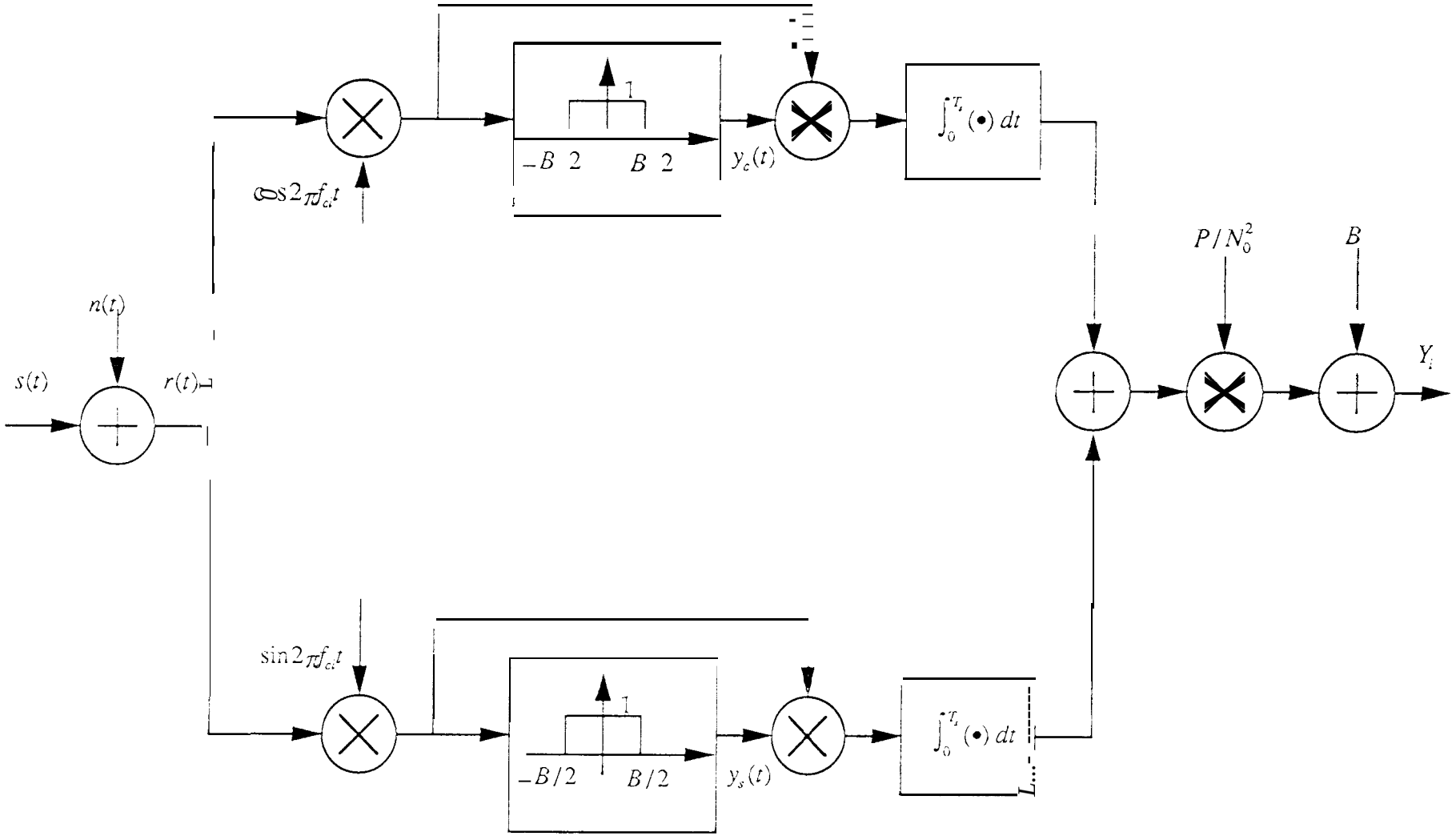

Fig. 6a. Channel i Noncoherent Processor for Low SNR ALR Receiver

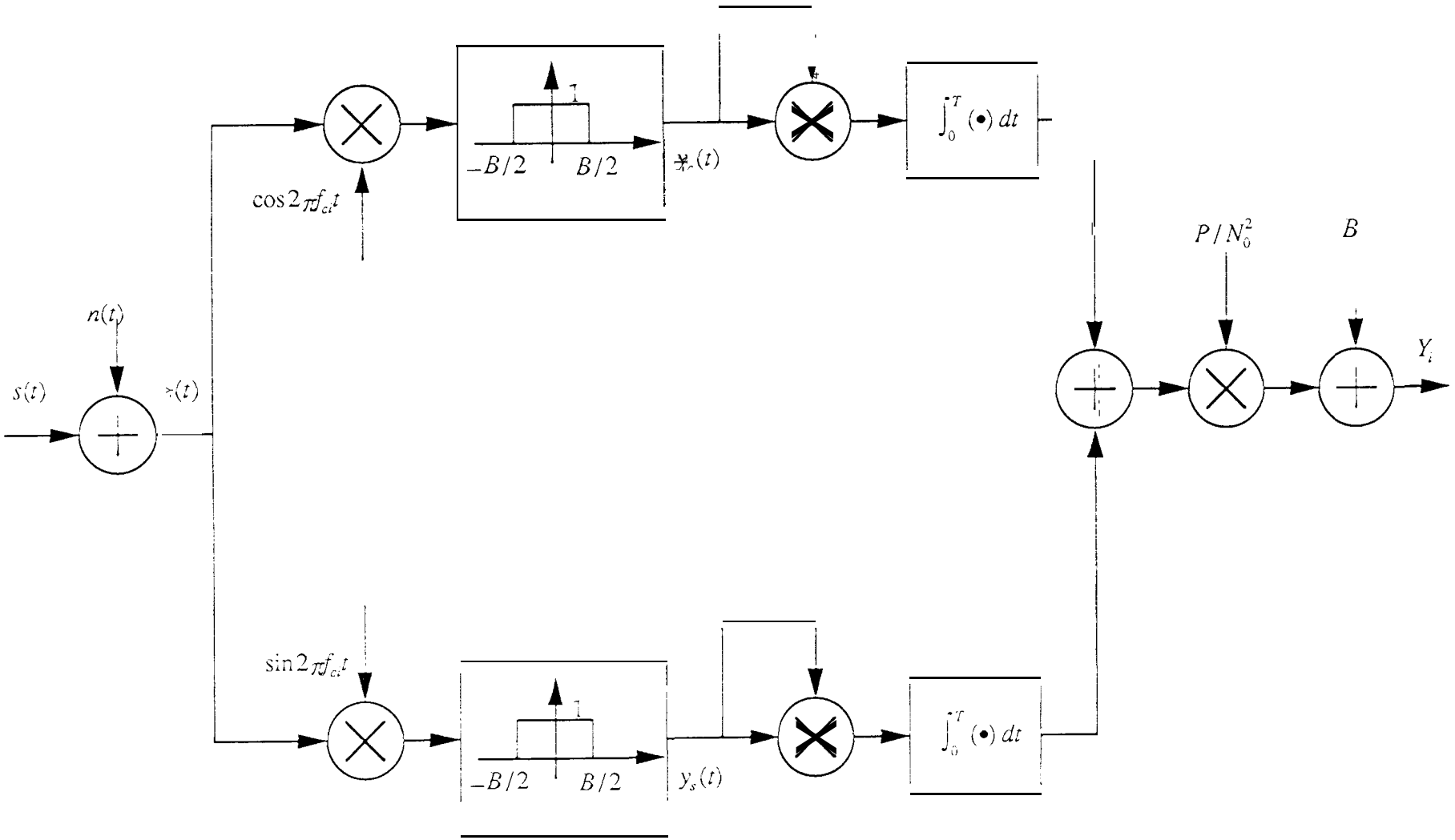

Fig. 6b. An Alternate Channel *i* Noncoherent Processor for Low SNR ALR Receiver

Figure 7.

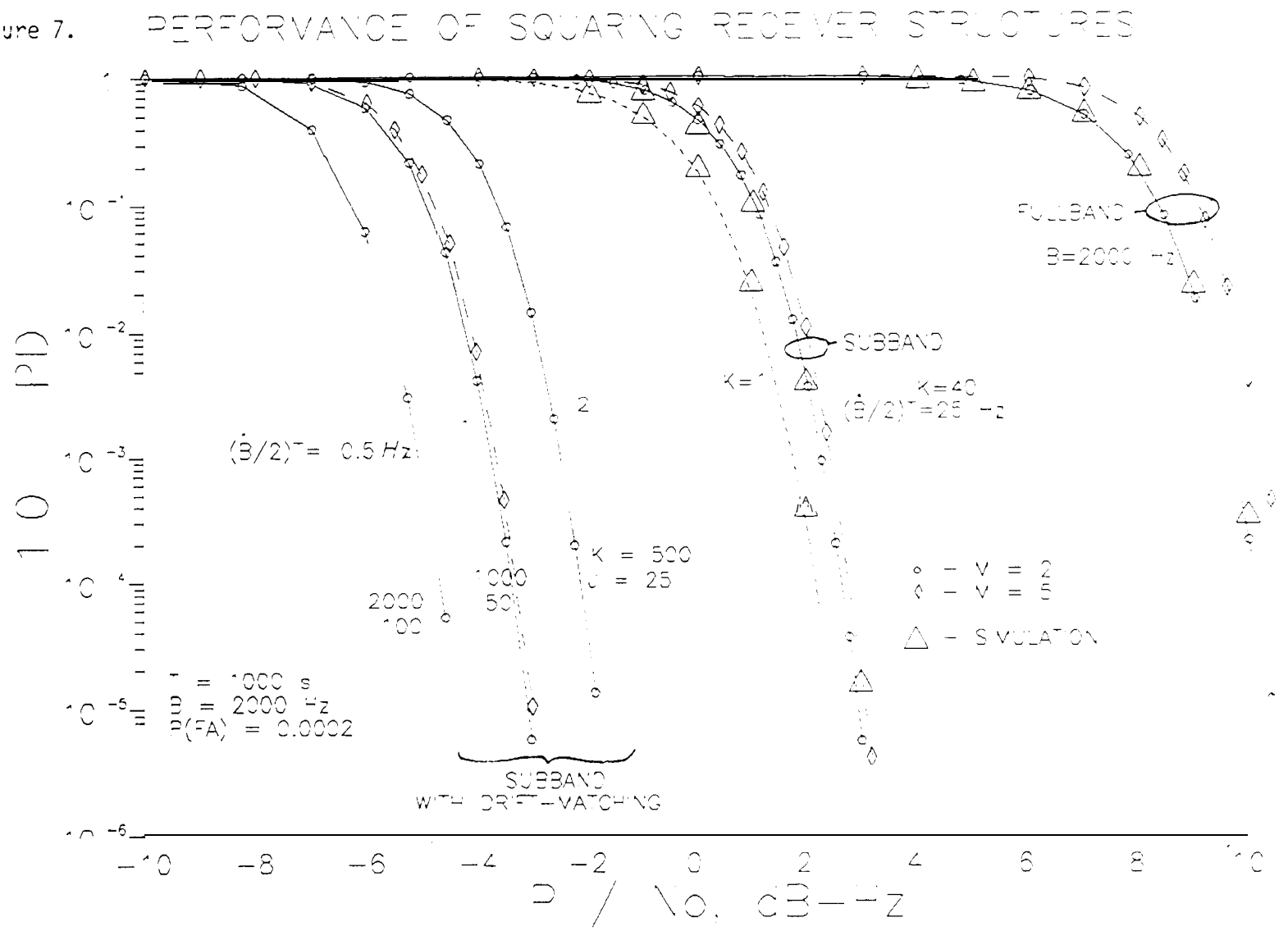
PERFORMANCE OF SQUARING RECEIVER STRUCTURES
FULLBAND
B=2000 Hz
SUBBAND
K=40
(B/2)T=25 Hz
(B/2)T= 0.5 Hz
K = 500
= 25
2000
100
1000
50
° - V = 2
◇ - V = 5
△ - SIMULATION
T = 1000 s
B = 2000 Hz
P(FA) = 0.0002
SUBBAND
WITH DRIFT-MATCHING
P(D)
D / NO, dB-Hz

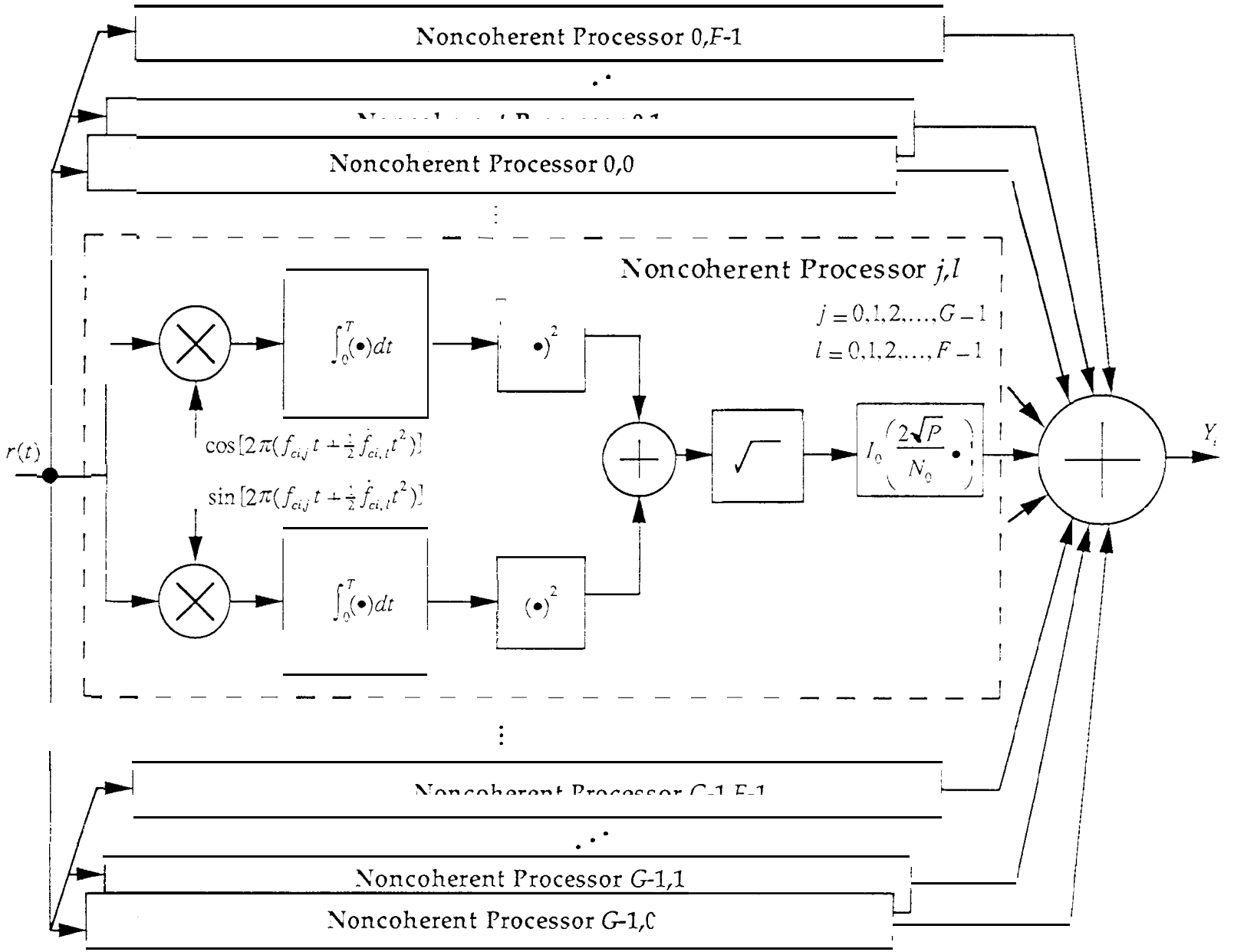

Fig. 8. Channel i ALR Detector for Detection of M-1 Sinusoidal Tones with Unknown Phase, Frequency, and Frequency Rate in AWGN

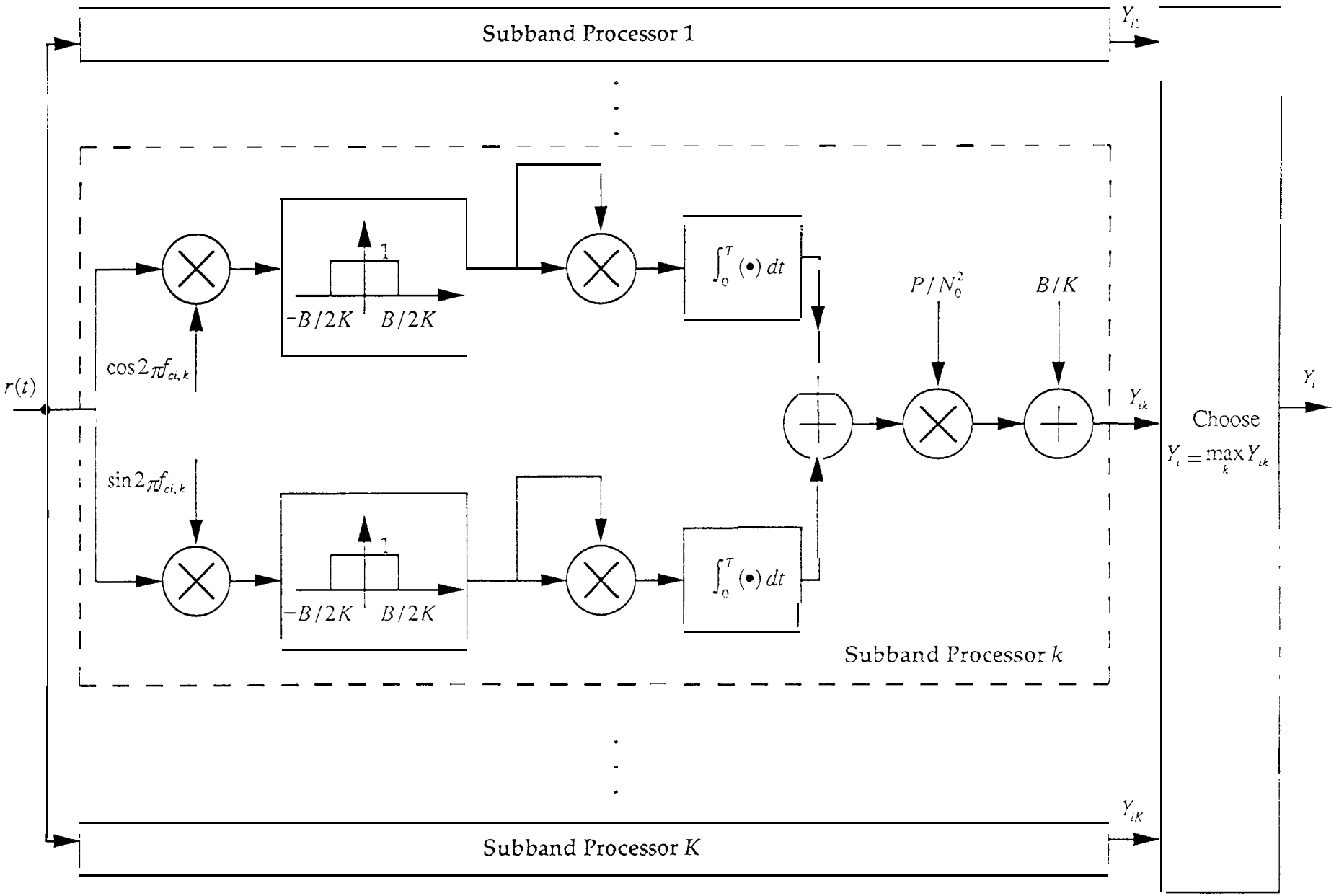

Fig. 9. Channel i Noncoherent Processor for Subband Receiver

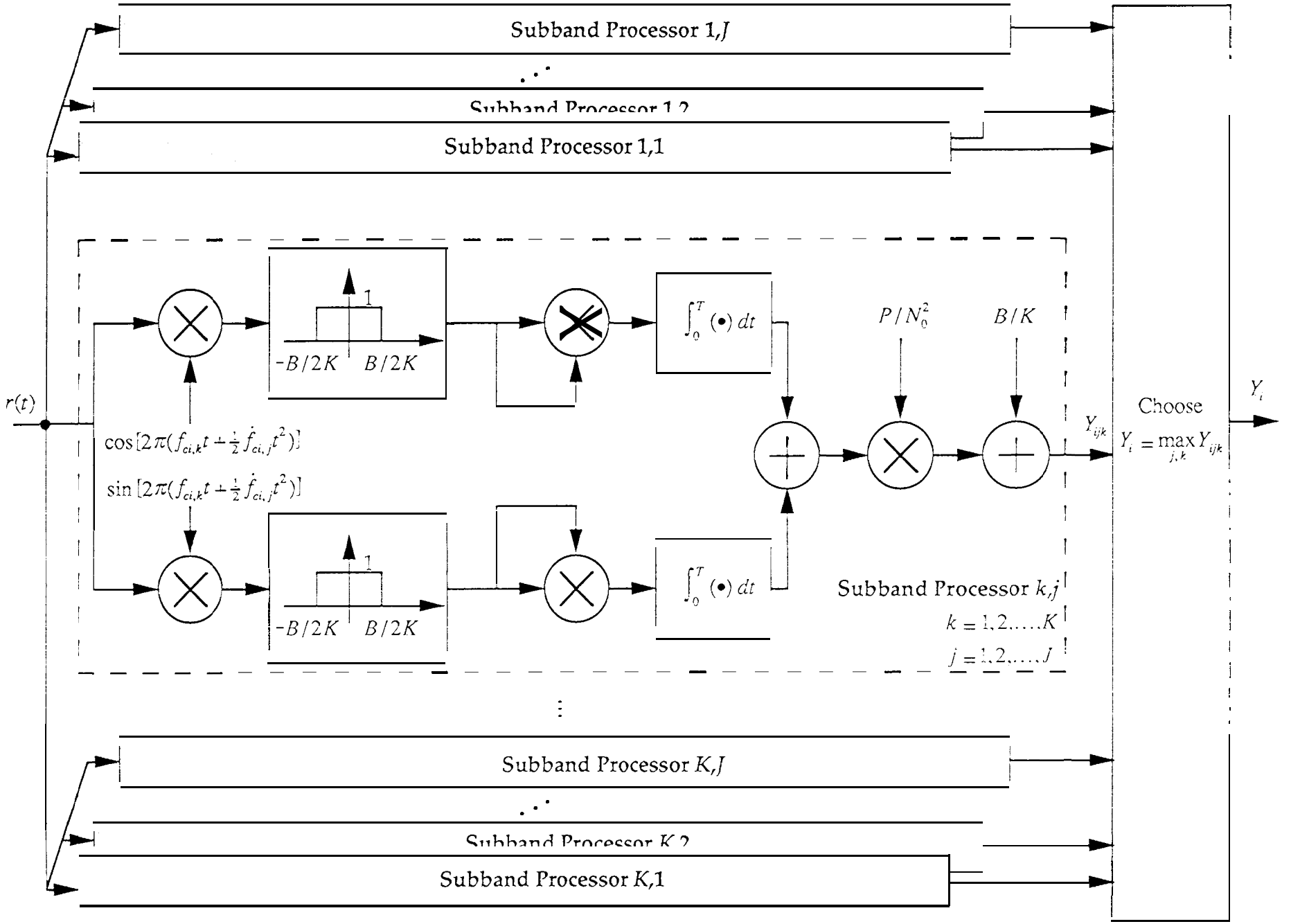

Fig. 10. Channel i Noncoherent Processor for Subband Drift Matching Receiver